

Computational methods on tool forces in friction stir welding

***Z. Zhang, Q. Wu, and H.W. Zhang**

State Key Laboratory of Structural Analysis for Industrial Equipment, Department of Engineering Mechanics, Faculty of Vehicle Engineering and Mechanics, Dalian University of Technology, Dalian 116024, China

*Corresponding author: zhangz@dlut.edu.cn

Abstract

The commercial applications of friction stir welding (FSW) to hard materials are limited by tool breakages. But the tool forces and the relations to tool geometries remain unknown. So, here we established a model on calculation of tool forces in FSW and examined how the tool design affects the temperature fields and the tool forces along the welding direction. Results indicate that temperature rises are very important for the tool forces in FSW. Both the increase of the shoulder size and the increase of the rotating speed can lead to the increase of the welding temperatures in FSW and then decrease the tool forces in the welding direction. Larger shoulder or higher rotating speed can increase the tool life.

Keywords: Friction stir welding, Finite element method, Tool force, Temperature

Introduction

Friction stir welding (FSW) has been invented for more than 15 years. Due to its solid joining nature, FSW has many advantages over the traditional fusion welding techniques, such as low distortion, low welding defects, fine grains in welding zone, etc., which makes it being successfully applied to aerospace, automobile, ship industries, etc. In FSW, a rotating tool is inserted into the butt of two welding plates and then translates along the welding line [Thomas et al. (1991); Mishra and Ma (2005)]. Based on the principles for FSW, friction stir processing (FSP) was developed by [Berbon et al. (2001)] as a genetic tool for microstructural modifications. FSW has been used for the joining of aluminum alloys [Ahmed et al. (2008); Altenkirch et al. (2008); Nielsen (2008); Fonda et al. (2008); Cabibbo et al. (2007)], magnesium alloys [Afrin et al. (2008); Gharacheh et al. (2006); Park et al. (2003)], stainless steels [Reynolds et al. (2003); Saeid et al. (2008)], titanium alloys [Mironov et al. (2008); Lee et al. (2005)], copper alloys [Park et al. (2004)], composite materials [Feng et al. (2008); Fernandez et al. (2004)] and even the joining of dissimilar materials [Kwon et al. (2008); Ouyang et al. (2006); Cavaliere et al. (2009)]. During the welding process, welding tool is believed to be the key component for a successful FSW [Elangovan et al. (2008); Zhang et al. (2009); Kumar and Kailas (2008)], especially for FSW of strong material [Bhadeshia and DebRoy (2009)]. Although the tool force in welding direction can be measured in experiments [Yan et al. (2005)], the theories for determination of the tool forces in FSW should be needed for the development of reliable, lasting and cost effective welding tools and even for the optimization of welding tools with lower costs. So, here we presented a method for calculation of tool forces. Temperature rises are believed to be one of the key factors to affect the plasticized material flow near the welding tool [Zhang and Zhang (2009); Nandan et al. (2007)]. So, the calculated tool forces, the temperature rises and the different tools are considered together for the examination on how the tool design affects the temperature fields and the tool forces along the welding direction.

Model description

ABAQUS was used with the combination of the user subroutine which was compiled by FORTRAN code for the description of a modified coulomb friction law [Zhang (2008)]. Eight node

thermo-mechanical brick elements are used for the mesh generation of the workpiece. For convenience of mesh generation with brick elements, a circular workpiece with the radii of 30mm is considered. The model has been validated for the temperature and material flow during FSW of AA6061 [Zhang and Zhang (2008); Zhang et al. (2011); Zhang and Zhang (2007); Zhang and Zhang (2009)]. The applied axial pressure is selected to be 70MPa, the pre-heating time 1.5s and the traverse speed 140mm/min for the current computations. The inflow temperature is set to be the room temperature (25°C). The boundary of the welding plate is treated as Eulerian type, on which the motion of the material points can be independent of the meshes. Arbitrary Lagrangian—Eulerian (ALE) method [Belytschko et al. (2000)] is combined with the adaptive meshing to avoid excessive element distortions. Four different tool profiles are used for the numerical comparisons, as shown in Fig.1. For the tool with a shoulder diameter of 20mm, three rotating speeds, i.e. 500rpm, 550rpm and 600rpm are used to study the effect of rotating speed on tool force. For other cases, the rotating speed is set to be 500rpm.

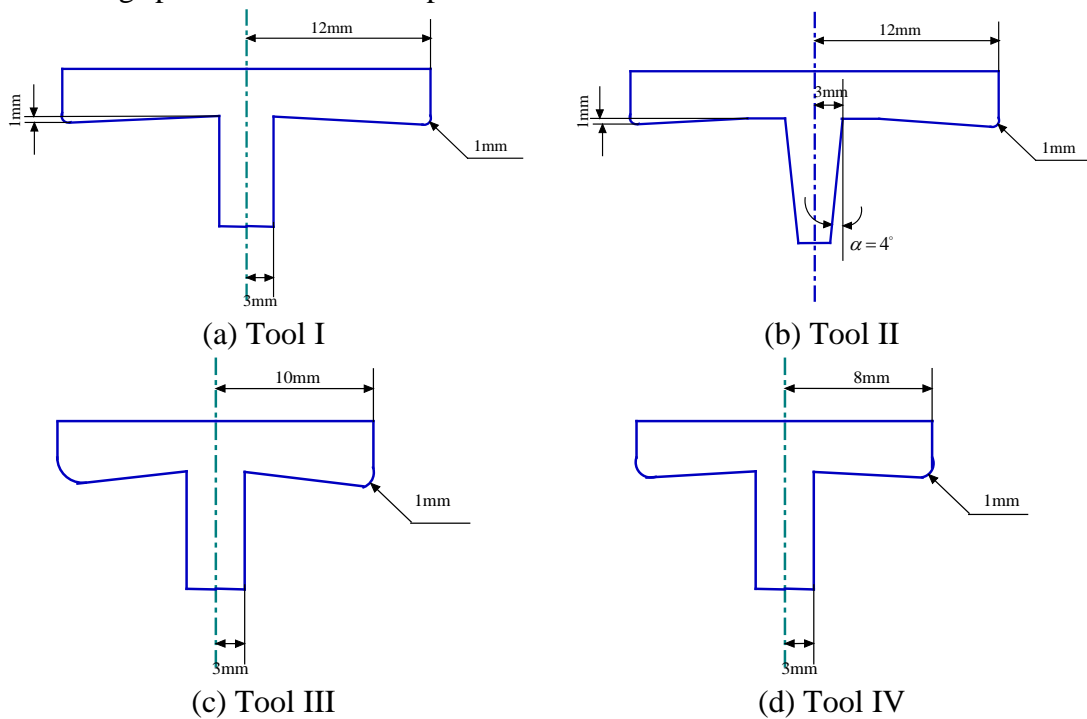


Figure 1 Schematics of welding tools

As shown in Fig.2, the tool forces in FSW can be determined by the hydraulic pressure and the frictional stresses on contact surfaces,

$$F_{\text{Long}} = \int_{S_1} p \sin \theta dS_1 + \int_{S_1} p_t \cos \theta dS_1 + \int_{S_2} p_t dS_2 \quad (1)$$

where p is the hydraulic pressure and p_t frictional stress. S_1 and S_2 are the pin-plate contact area and the shoulder-plate contact area, respectively.

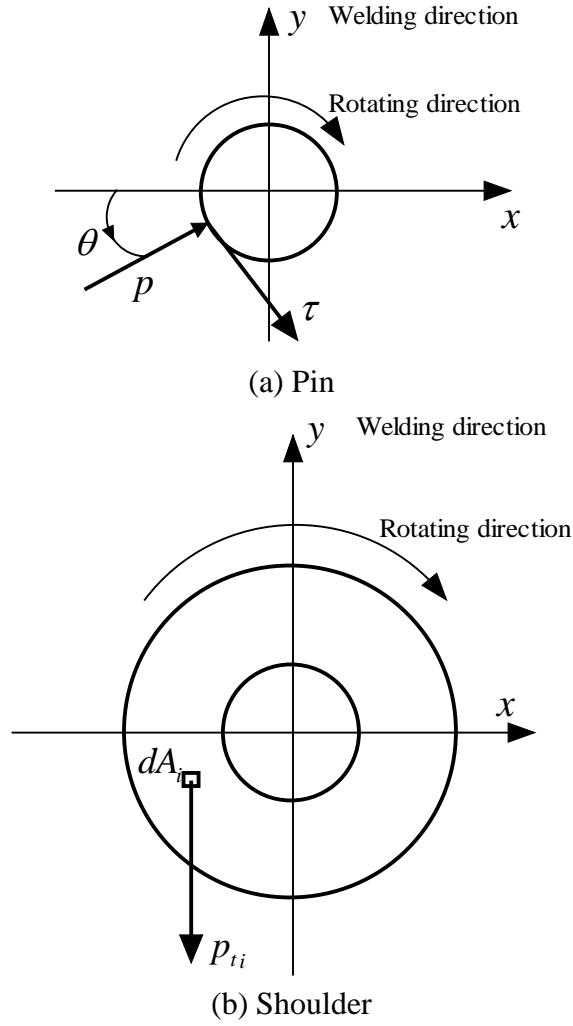


Figure 2 Calculation of tool forces in FSW

The hydraulic pressure can be obtained from the trace of the stress tensor in FSW,

$$p = -\frac{1}{3} \text{trace}(\sigma_{ij}) \quad (2)$$

where σ_{ij} is the Cauchy stress tensor which can be computed using the constitutive equation,

$$\sigma_{ij} = C_{ijkl} \varepsilon_{kl}^e \quad (3)$$

where C_{ijkl} is the elasticity tensor and ε_{kl}^e is the elastic part of the strain ($\varepsilon_{kl} - \varepsilon_{kl}^p$). The total strain can be computed using the strain displacement equation,

$$\varepsilon_{ij} = \frac{1}{2} (u_{i,j} + u_{j,i}) \quad (4)$$

where u_i is the displacement. The boundary condition used for the inflow and outflow regions are $u_i=0$ for $i=2, 3$ and $u_{i,t}=140\text{mm/s}$ for $i=1$.

The predictor-corrector method is used for the calculations of the plastic strain,

$$\dot{\varepsilon}^p = \dot{\lambda} \frac{3\sigma'}{2\sigma} \quad (5)$$

where λ is the plastic rate parameter, σ is the deviatoric stress, and $\bar{\sigma}$ is the von Mises effective stress. The yield function can be defined as,

$$f = \bar{\sigma} - \sigma_s(T) = 0 \quad (6)$$

where σ_s is the yield stress which is the function of temperature.

The temperature is determined by solving the heat transfer equation

$$\rho c \frac{\partial T}{\partial t} - \frac{\partial}{\partial x} \left(k \frac{\partial T}{\partial x} \right) - \frac{\partial}{\partial y} \left(k \frac{\partial T}{\partial y} \right) - \frac{\partial}{\partial z} \left(k \frac{\partial T}{\partial z} \right) - \rho Q = 0 \quad (7)$$

$$k \frac{\partial T}{\partial x} n_x + k \frac{\partial T}{\partial y} n_y + k \frac{\partial T}{\partial z} n_z = q \quad (8)$$

where ρ is the density, c is the specific heat, k is the thermal conductivity, q is the heat flux on the contact area and n_x, n_y, n_z represent the directions. The temperature dependent values of c and k can be found in [An and Liu (1998)]. Q is the heat generated by the plastic deformations,

$$Q = \sigma_{ij} \dot{\epsilon}_{ij}^p \quad (9)$$

where $\dot{\epsilon}_{ij}^p$ is the strain rate.

The heat flux on the contact area q is,

$$q = \eta p_t \dot{\gamma} \quad (10)$$

where η is the fraction of frictional heat entering the workpiece (90% in current work), $\dot{\gamma}$ is the relative velocity between the tool and workpiece.

The general finite element form for the heat transfer equation can be obtained by the spatial discretization,

$$C\dot{T} + KT = P \quad (11)$$

where C is the heat capacity matrix, K the thermal conductivity matrix and P is the thermal load matrix which is determined by the mentioned internal heat source, the heat flux on contact surface and the boundary conditions. Explicit forward difference integration method is used to solve this equation.

The displacement required to compute total strain can be determined solving the equation of motion,

$$\sigma_{ij,j} + F_i = \rho u_{i,tt} \quad (12)$$

where F_i is the body force per unit volume and $u_{i,tt}$ is the acceleration.

The classical finite element form of the above equations can be obtained by spatial discretization,

$$M\ddot{u} = P' - P'_{int} \quad (13)$$

where M is the mass matrix, P' load matrix and P'_{int} internal nodal forces. Explicit central difference integration method is used for the computation of displacements and accelerations of nodes. The load matrix consists of the contact forces, normal (p_n) and tangent (p_t). The contact forces can be expressed in terms of displacements of the contact points by the penalty algorithm [Zhang et al. (2005)] with consideration of the shear failure criterion,

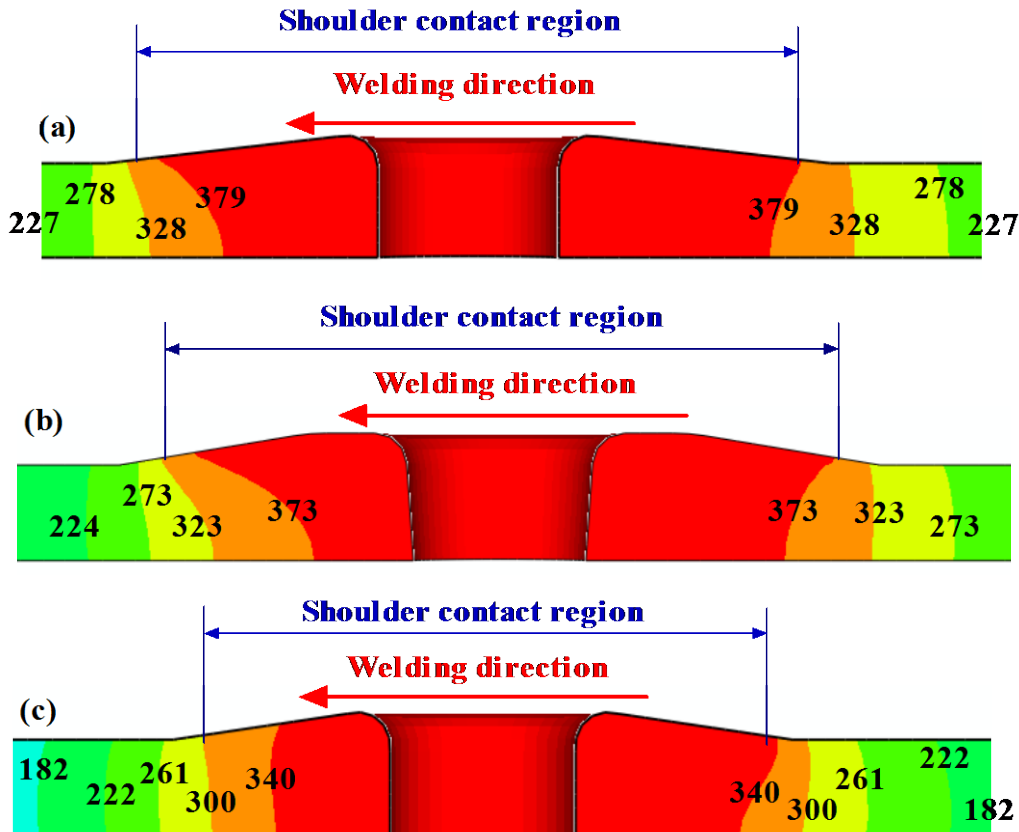
$$p_n = -E_n (du_n^s - du_n^m - \delta^*) \text{ for both sliding and sticking states} \quad (14)$$

$$p_t = -\min(\mu p_n \text{sign}(du_t^s - du_t^m), \sigma_s / \sqrt{3}) \text{ for sliding state} \quad (15)$$

where E_n is penalty factor for normal contact, which can be taken from 1 to 100 times of the element stiffness of the representative underlying welding material according to the overclosures in calculations. δ^* is the gap. du_n is the normal displacement. The superscripts m and s represent the mater (tool) and slave (welding plate) contact surfaces. The displacement for master is considered to be zero in this calculation.

Results and discussions

The computed temperature fields around the tool are shown in Fig. 3. The maximum temperature for Tool I in 500rpm and 140mm/min is 430 °C, as shown in Fig. 3(a). The experimental measured temperature is about 440 °C under the same welding conditions and tool sizes [Chen and Kovacevic (2003)], which can verify the developed model for heat transfer. When conical pin is used, the maximum temperature is decreased slightly to 426 °C, as shown in Fig. 3(b). Compared with the variation of pin shape, the effect of shoulder size on temperature is more obvious. When the shoulder radius is changed to 10mm, the maximum temperature is decreased to 384 °C, as shown in Fig. 3(c). With the further decrease of the shoulder radius to 8mm, the maximum temperature can be further decreased to 344 °C, as shown in Fig. 3(d). The observation on effect of shoulder size on temperature is consistent to previous studies [Zhang et al. (2009)]. Usually, higher rotating speed is used for smaller shoulder. So, two new cases for Tool III (Fig. 1) with higher rotating speeds are adopted for comparisons. When the rotating speed is increased to 550rpm, the maximum temperature can be increased to 393 °C, as shown in Fig. 3(e). With the further increase for the rotating speed to 600rpm, the maximum temperature can be increased to 400 °C, as shown in Fig. 3(f).



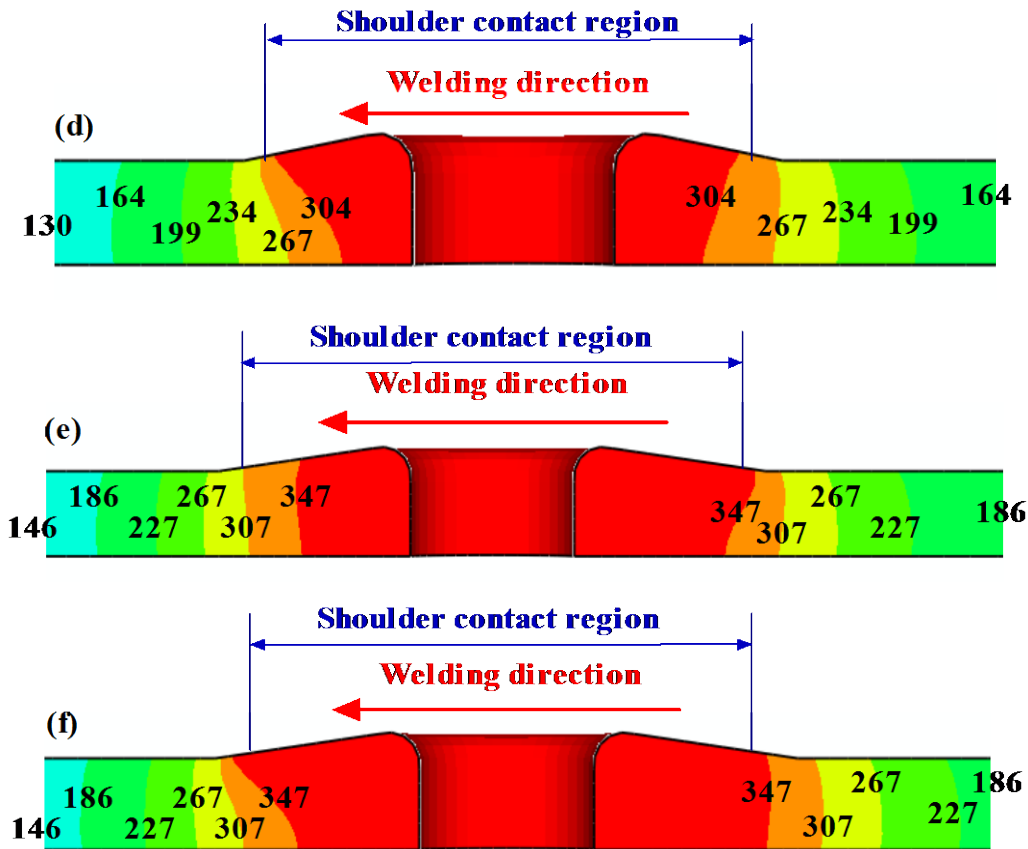


Figure 3 Temperatures in different cases: (a) Tool I in 500rpm ($T_{\max} = 430^{\circ}C$); (b) Tool II in 500rpm ($T_{\max} = 426^{\circ}C$); (c) Tool III in 500rpm ($T_{\max} = 384^{\circ}C$); (d) Tool IV in 500rpm ($T_{\max} = 344^{\circ}C$); (e) Tool III in 550rpm ($T_{\max} = 393^{\circ}C$); (f) Tool III in 600rpm ($T_{\max} = 400^{\circ}C$)

Temperature fields are important for the plasticization of the material near the welding tool. So, it can significantly affect the frictional force calculation and even the tool forces. Frictional stresses along selected paths A=>B=>C are shown in Fig.4 for different cases. The frictional stress on the selected path is very similar for Tool I and Tool II. When the conical pin is adopted, the friction stress on the contact surface is increased slightly. The friction stress can be increased due to the decrease of the shoulder diameter and the decrease of the rotating speed. With consideration of the temperature fields shown in Fig.3, the frictional stress can be increased with the decrease of temperature in FSW. Moreover, the frictional stress on shoulder-plate interface is lower than the one on the pin-plate interface. But with the increase of the temperature due to the increase of rotating speed or increase of shoulder size, the friction stresses on pin-plate and shoulder-plate interfaces become similar.

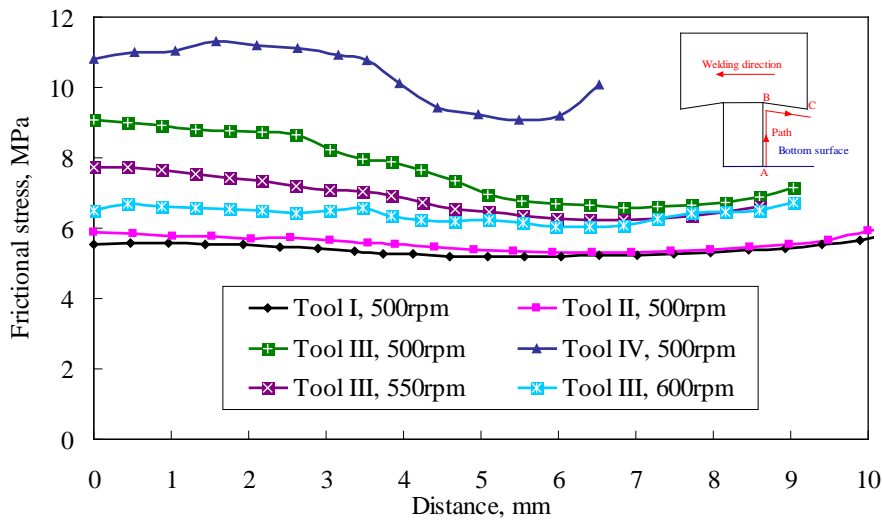


Figure 4 Comparison of frictional stress in different cases

The calculated forces for different cases are shown in Fig. 5. When Tool I with 500rpm is used, the calculated force in welding direction is 3.4kN. But when conical pin is adopted under the same welding conditions, the tool force in welding direction is increased to 4kN due to the decrease of temperature. When smaller shoulders are used for Tool III and Tool IV, the tool forces in welding direction is obviously increased due to the obvious decrease of temperatures. This is the reason that the larger shoulder can increase the tool life in manufacture. The experimentally measured transverse force is about 8kN under the rotating speed of 500rpm and the shoulder diameter of 20.3mm for FSW of AA2524 [Yan et al. (2005)]. In fact, AA6061 can be believed to be softer than AA2524 due to the smaller yield stress. So, it can be deduced that the transverse force for FSW of AA6061 should be smaller than the one in FSW of AA2524 under the similar welding conditions. For Tool III in 500rpm, the transverse force in FSW of AA6061 is 6.5kN. The comparison with Ref. [Yan et al. (2005)] shows that the computed transverse force in current model is reasonable. For smaller shoulder (Tool III), the increase of the rotating speed can decrease the tool force in welding direction apparently. This means that higher rotating speed should be used in manufacture for smaller shoulder in FSW, which can lead to more temperature rises. With the increase of the temperature, the material becomes softer and then the tool force in welding direction can be decreased.

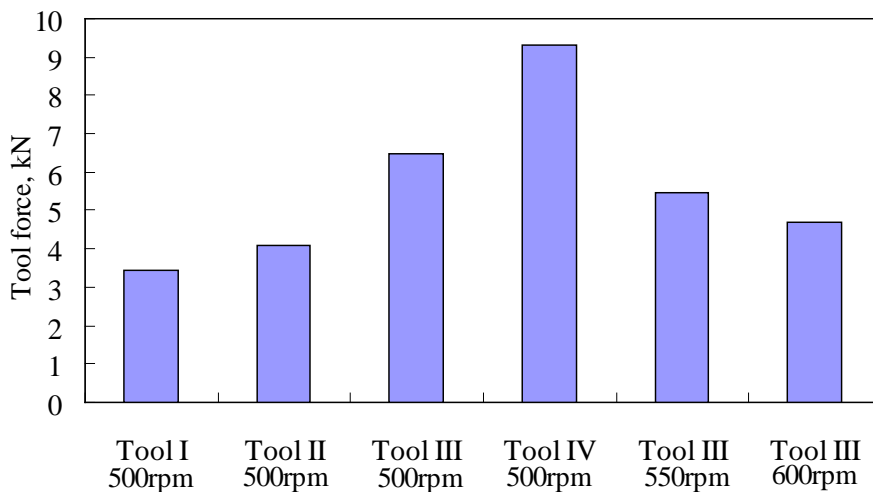


Figure 5 Tool forces in welding direction in different cases

Conclusions

- 1) Temperature rise is very important for the tool force in FSW. Higher temperature can lead to softer material near the welding tool and the decrease the tool forces in welding direction.
- 2) Both the increase of the shoulder size and the increase of the rotating speed can lead to the increase of the temperatures in FSW and then decrease the tool forces in welding direction.
- 3) Larger shoulder or higher rotating speed can increase the tool life.

Acknowledgement

This work was supported by Program for New Century Excellent Talents in University, the Fundamental Research Funds for the Central Universities, the National Natural Science Foundation of China (Nos. 11172057 and 11232003), the National Key Basic Research Special Foundation of China (2011CB013401) and the National High Technology Research and Development Program of China (2012AA050901).

References

- W.M. Thomas, E.D. Nicholas, J.C. Needham, M.G. Murch, P. Templesmith, C.J. Dawes. Friction stir welding, International Patent Application No. PCT/GB92102203 and Great Britain Patent Application No. 9125978.8, 1991.
- R.S. Mishra, Z.Y. Ma. Friction stir welding and processing, *Materials Science and Engineering R*, 2005, 50:1-78.
- P.B. Berbon, W.H. Bingel, R.S. Mishra, C.C. B.M.W. Mahoney. Friction stir processing: a tool to homogenize nanocomposite aluminum alloys, *Scripta Materialia*, 2001, 44: 61-66.
- M.M.Z. Ahmed, B.P. Wynne, W.M. Rainforth, P.L. Threadgill. Quantifying crystallographic texture in the probe-dominated region of thick-section friction-stir-welded aluminium, *Scripta Materialia*, 2008, 59: 507-510.
- J. Altenkirch, A. Steuwer, M. Peel, D.G. Richards, P.J. Withers. The effect of tensioning and sectioning on residual stresses in aluminium AA7749 friction stir welds, *Materials Science and Engineering A*, 2008, 488: 16-24.
- K.L. Nielsen. Ductile damage development in friction stir welded aluminum (AA2024) joints, *Engineering Fracture Mechanics*, 2008, 75: 2795-2811.
- R.W. Fonda, K.E. Knippling, J.F. Bingert. Microstructural evolution ahead of the tool in aluminum friction stir welds, *Scripta Materialia*, 2008, 58: 343-348.
- M. Cabibbo, H.J. McQueen, E. Evangelista, S. Spigarelli, M. Di Paola, A. Falchero. Microstructure and mechanical property studies of AA6056 friction stir welded plate, *Materials Science and Engineering: A*, 2007, 460-461: 86-94.
- N. Afrin, D.L. Chen, X. Cao, M. Jahazi. Microstructure and tensile properties of friction stir welded AZ31B magnesium alloy, *Materials Science and Engineering A*, 2008, 47: 179-186.
- M. Abbasi Gharacheh, A.H. Kokabi, G.H. Daneshi, B. Shalchi, R. Sarrafi. The influence of the ratio of “rotational speed/traverse speed” (ω/v) on mechanical properties of AZ31 friction stir welds, *International Journal of Machine Tools and Manufacture*, 2006, 46: 1983-1987.
- S.H.C. Park, Y.S. Sato, H. Kokawa. Effect of micro-texture on fracture location in friction stir weld of Mg alloy AZ61 during tensile test, *Scripta Materialia*, 2003 49: 161-166.
- A. P. Reynolds, W. Tang, T. Gnaupel-Herold, H. Prask. Structure, properties, and residual stress of 304L stainless steel friction stir welds, *Scripta Materialia*, 2003, 48: 1289-1294.
- T. Saeid, A.A.H. Assadi, F.M. Ghaini. Effect of friction stir welding speed on the microstructure and mechanical properties of a duplex stainless steel, *Materials Science and Engineering A*, 2008, 496: 262-268.
- S. Mironov, Y. Zhang, Y.S. Sato, H. Kokawa. Crystallography of transformed β microstructure in friction stir welded Ti-6Al-4V alloy, *Scripta Materialia*, 2008, 59: 511-514.
- W.B. Lee, C.Y. Lee, W.S. Chang, Y.M. Yeon, S.B. Jung. Microstructural investigation of friction stir welded pure titanium, *Materials Letters*, 2005, 59: 3315-3318.
- H.S. Park, T. Kimura, T. Murakami, Y. Nagano, K. Nakata, M. Ushio. Microstructures and mechanical properties of friction stir welds of 60% Cu-40% Zn copper alloy, *Materials Science and Engineering A*, 2004, 371: 160-169.
- A.H. Feng, B.L. Xiao, Z.Y. Ma. Grain boundary misorientation and texture development in friction stir welded SiCp/Al-Cu-Mg composite, *Materials Science and Engineering A*, 2008, 497: 515-518.
- G.J. Fernandez, L.E. Murr. Characterization of tool wear and weld optimization in the friction-stir welding of cast aluminum 359+20% SiC metal-matrix composite, *Materials Characterization*, 2004, 52: 65-75.
- Y.J. Kwon, I. Shigematsu, N. Saito. Dissimilar friction stir welding between magnesium and aluminum alloys, *Materials Letters*, 2008, 62: 3827-3829.
- J. Ouyang, E. Yarrapareddy, R. Kovacevic. Microstructural evolution in the friction stir welded 6061 aluminum alloy (T6-temper condition) to copper, *Journal of Materials Processing Technology*, 2006, 172: 110-122.
- P. Cavaliere, A. De Santis, F. Panella, A. Squillace. Effect of welding parameters on mechanical and microstructural properties of dissimilar AA6082-AA2024 joints produced by friction stir welding, *Materials & Design*, 2009, 30: 609-616.

- K. Elangovan, V. Balasubramanian. Influences of tool pin profile and welding speed on the formation of friction stir processing zone in AA2219 aluminium alloy, *Journal of Materials Processing Technology*, 2008, 200: 163-175.
- Z. Zhang, Y.L. Liu, J.T. Chen. Effect of shoulder size on the temperature rise and the material deformation in friction stir welding, *International Journal of Advanced Manufacturing Technology*, 2009, 45: 889-895.
- K. Kumar, S.V. Kailas. The role of friction stir welding tool on material flow and weld formation, *Materials Science and Engineering A*, 2008, 485: 367-374.
- H.K.D.H. Bhadeshia, T. DebRoy. Critical assessment: friction stir welding of steels, *Science and Technology of Welding and Joining*, 2009, 14(3): 193-196.
- J.H. Yan, M.A. Sutton, A.P. Reynolds. Process—structure—property relationships for nugget and heat affected zone regions of AA2524—T351 friction stir welds, *Science and Technology of Welding and Joining*, 2005, 10(6): 725-736.
- Z. Zhang, H.W. Zhang. Numerical studies on controlling of process parameters in friction stir welding, *Journal of Materials Processing Technology*, 2009, 209(1): 241-270.
- R. Nandan, G.G. Roy, T.J. Lienert, T. Debroy. Three-dimensional heat and material flow during friction stir welding of mild steel, *Acta Materialia*, 2007, 55: 883-895.
- Z. Zhang. Comparison of two contact models in the simulation of friction stir welding process, *Journal of Materials Science*, 2008, 43: 5867-5877.
- Z. Zhang, H.W. Zhang. A fully coupled thermo-mechanical model of friction stir welding, *International Journal of Advanced Manufacturing Technology*, 2008, 37: 279-293.
- Z. Zhang, J.T. Chen, Z.W. Zhang, H.W. Zhang. Coupled thermo-mechanical model based comparison of friction stir welding processes of AA2024-T3 in different thicknesses, *Journal of Materials Science*, 2011, 46: 5815-5821.
- Z. Zhang, H.W. Zhang. Numerical studies of pre-heating time effect on temperature and material behaviors in friction stir welding process, *Science and Technology of Welding and Joining*, 2007, 12(5): 436-448.
- Z. Zhang, H.W. Zhang. Numerical studies on the effect of transverse speed in friction stir welding, *Materials & Design*, 2009, 30: 900-907.
- T. Belytschko, W.K. Liu, B. Moran. *Nonlinear finite elements for continua and structures*, John Wiley & Sons, Ltd, New York, 2000.
- J.R. An, Y.H. Liu. *Handbook of Chinese and foreign metals materials most in use*, Xi'an: Shanxi Science and Technology Press, 1998. (in Chinese)
- H.W. Zhang, H. Wang, P. Wriggers, B.A. Schrefler. A finite element model for contact analysis of multiple Cosserat bodies, *Computational Mechanics*, 2005, 36(6): 444-458.
- C.M. Chen, R. Kovacevic. Finite element modeling of friction stir welding—thermal and thermomechanical analysis, *International Journal of Machine Tools and Manufacture*, 2003, 43: 1319-1326.